Preferential geometry of a Peptide-Perylenediimide derivative dimer for a targeted self-assembly

5.1 INTRODUCTION

Non-covalent forces are key factors for supramolecular self-assemblies relevant to biological systems or material sciences [Müller-Dethlefs and Hobza, 2000; Ebrahimi *et al.*, 2014]. The monomer units or fragments of molecules are linked to each other via hydrogen bonds, $\pi - \pi$ stacking, hydrophobic interactions to create a self-assembled organization of molecules important in crystal engineering, protein folding, drug-binding and in designing molecular devices [Israelachvili *et al.*, 1977; Sinnokrot and Sherrill, 2006]. Out of these non-covalent interactions, the stacking interactions play an important role in the field of biology and have immense applications in material sciences. Different types of stacking between two aromatic moieties are reported such as cation, anion or C-H-π interactions [Vijay and Sastry, 2010; Mahadevi and Sastry, 2016]. For example, the drug Aricept, which is an anti-Alzeheimers drug involves O-H/π and cation stacking [Meyer *et al.*, 2003]. In DNA, the stacking interactions between two base pairs and hydrogen bonding between the two DNA strands are responsible for the stability of DNA helical structure [Fonseca Guerra *et al.*, 1999]. π-interactions are found to be important in organic electronic devices as they possess semi-conducting properties [Engelkamp *et al.*, 1999; Würthner, 2004]. Perylenediimide ring systems (PDI) have shown their usefulness in solar devices, diodes and transistors [Ahmed *et al.*, 2017; Spillmann *et al.*, 2009; Pramanik *et al.*, 2017; Ahmed *et al.*, 2018]. Thus, understanding the role of non-covalent interactions on the stability of the self-assembled systems and then finding the molecular structure key to the tailor made nano-structures are topics of interests in its own right. Experimental analysis of $\pi - \pi$ interaction becomes complex in systems which involve solvent effects and secondary interactions [Sinnokrot and Sherrill, 2006].

Recent progresses on computational chemistry make it easier to identify the type of stacking involved in the system. The intersheet binding energies computed for both sandwiched and slipped parallel polyaromatic hydrocarbon sheets (PAHs) using SOS-MP2 method are in good agreement with the experiments [Silva *et al.*, 2016]. Density functional theory (DFT) in presence of dispersion corrections is used to study $\pi - \pi$ interactions between heterocyclic aromatic compounds with benzene molecules. A notable contribution of dispersion forces is found to the energy of the optimized parallel stacked arrangement [Oltean *et al.*, 2013]. Electrostatic factors are found to contribute in the orientation of aromatic rings [Huber *et al.*, 2014]. DFT based studies have been conducted on dimer systems with PDI core and relations have been established between their geometry, binding energy and their electronic coupling [Vura-Weis *et al.*, 2010]. MD simulations of multimeric Perylenediimide-DNA surrogates show that the assemblies of these multimeric structures are highly dependent on the van der Waals and electrostatic interactions [Markegard *et al.*, 2015]. Replica exchange MD simulations of DNA adsorption on the surface of graphene oxide shows that the $\pi - \pi$ stacking and hydrogen bonding play roles in the adsorption phenomena [Xu *et al.*, 2017]. Thermodynamic and kinetic factors are known to play important roles in tuning sugar-based perylene- diimide derivative PTCDI-BAG structures and helicity [Hu *et al.*, 2012].

Self-assembly of a PDI-peptide conjugate (FF-PDI-FF, referred to as P-1) is reported earlier [Ahmed *et al.*, 2017, 2018] where P-1 forms right handed helical nano-fibres in THF (Tetrahydrofuran). The nano-fibres change to nanorings with left-handed helicity in 10%

THF-water. Combined results from the circular dichroism (CD) analysis and FESEM images show the formation of nano-fibres with right handed helicity in the presence of THF whereas left-handed nano-rings are formed when 10% THF-water solvent is used. Experimental results have shown the importance of kinetic and thermodynamic factors which control the self-assembly mechanism [Ahmed *et al.*, 2017]. It has been found that the nucleation stage for the formation of right handed helical fibres in THF solvent is a kinetically controlled process. On the other hand, the differential solubility in these two different solvents restrict the elongation of the fibre in 10% THF-water. This leads to a change in the helicity and the nanorings are formed. Thus tuning the super structure from right handed to left handed axial preference is achieved by their differential solubilities. This is of tremendous importance in organic electronic materials. At a THF concentration less than 20%, the absorption spectra of P-1 indicate the presence of $\pi - \pi$ stacking [Ahmed *et al.*, 2017]. To identify the building block and to understand the driving force that lead to such a specific super structure of nano-rings or helix, in this chapter, we first perform the electronic structure calculations for P-1 molecules. We show the effect of dispersion terms to the stacking behavior is significant. The most stable P-1 dimer with strongest binding energies from electronic structure calculations is used for MD simulations using water as the solvent. We identify the most stable geometry of the dimer from simulations and compared the structure characterized by UV-vis spectroscopy. Combining the electronic structure calculations and MD simulations we attempt to understand the preferential geometry of dimer in different solvents. We calculate the potential of mean force to identify the most stable geometry of the dimers in 10% THF-water concentration and in THF in a comprehensive manner. The study will enable to explain the formation of thermodynamically controlled left-handed nano-rings of P-1 [Ahmed *et al.*, 2017] under specific solvent conditions and will help in synthesizing soft materials with desired functionalities in future.

5.2 COMPUTATIONAL DETAILS

5.2.1 Electronic structure calculations

Geometry optimizations are carried out for a π-conjugated ring system, peptide-perylenediimide (P-1) (Phe-Phe motif and perylenediimide (PDI) core). Since there are large numbers of atoms in these molecules, the electronic structure calculation using density functional theory (DFT) involves a high computational cost. To avoid this, density functional tight binding (DFTB) method is implied in DFTB+ package [Aradi *et al.*, 2007; Koskinen and Mäkinen, 2009] to optimize the π-conjugated system. In DFT, the Kohn Sham method is followed for mapping the system of interacting electrons to a non-interacting electron system whose energy is given as,

$$E = T_s + E_{ext} + E_H + E_{XC} + E_{II} \tag{5.1}$$

where, T_s is the non-interacting kinetic energy, E_{ext} is the external interaction, E_H is the Hartree energy, E_{XC} is the exchange-correlation energy, and E_{II} is the ion-ion interaction energy. DFTB method uses minimal atom-centered basis sets and an approximate Hamiltonian based on DFT energy equation. So the computational cost is low and the time scales relevant to experiments are accessible. The DFTB Hamiltonian assumes a neutral and spherical charge distribution $n_0(r)$ along with self-consistent charges (SCC). The Kohn-Sham equation is expanded for energy E_n to second order charge fluctuation, δn. The total energy of the system is given by the equation,

$$E_{Tot} = E_{BS} + E_{coul}[\delta n] + E_{rep}(R) \tag{5.2}$$

where, E_{BS} is the band structure energy. The second energy term E_{Coul} arises due to the charge fluctuations which is mainly due to the Coulombic interactions, but it also contains the contributions from exchange-correlations. The third term E_{rep} denotes the repulsive energy due to the ion-ion repulsion. Following equation 5.2, a single molecule of PDI (figure 5.1 a) is first geometry optimized.
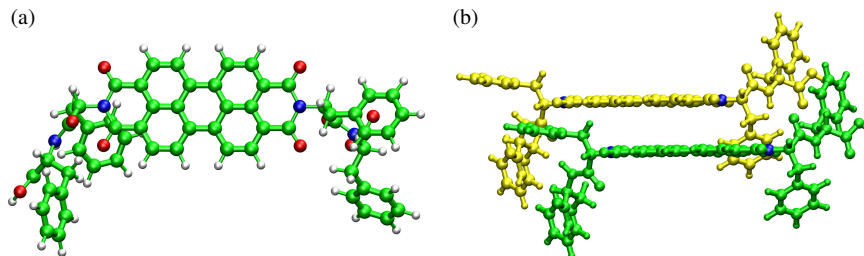
Figure 5.1: Snapshots of P-1 (a) monomer and (b) parallel slipped stacked dimer. Color codes: Red, oxygen; Green, carbon; Blue, nitrogen and White, hydrogen. For clarity, two monomers are shown in green and yellow and P-1 nitrogens are shown in blue.

Next, a stacked dimer of PDI is obtained by placing one geometry optimized PDI monomer on top of the other with an inter PDI-core distance of 3.5 Å and slipped by 3.8 Å and 4.4 Å along the core plane (x,y) (figure 5.1 (b)). The dimer is created to prepare the building blocks of left and right handed helices. A schematic representation of the left and right handed helices are shown in figure 5.2 (a) and (b) respectively. The angle between the vectors formed by joining the nitrogen atoms present at the two terminals of each PDI core is referred to as θ, the inter-planar angle, as shown in figure 5.3. The inter-planar angle between the two monomers of PDI is varied from -90° to 90° through an angle 0°. The parallel slipped stacked dimer with 0° inter-planar angle is shown in figure 5.1 (b). Positive and negative angles correspond to anti-clock wise and clock wise rotations respectively as followed in literature [Xu *et al.*, 2017] (figure 5.3 a) and b)). The binding energies
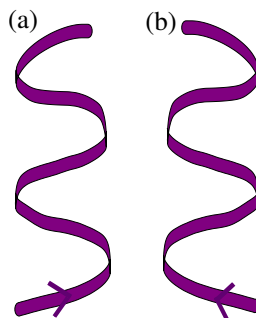

Figure 5.2: A schematic representation of (a) right handed helix (anticlockwise rotation) and (b) left handed helix (clockwise rotation). The orientations of the helices are similar as discussed in [Xu *et al.*, 2017].

of the stacked dimers are calculated using the following equation,

$$\Delta E_{BE} = E_{DE} - 2E_{ME} \tag{5.3}$$

where ΔE_{BE} is the binding energy, E_{DE} is the dimer energy and E_{ME} is the energy of the monomer. The binding energy of the fully optimized dimers using DFTB is shown in figure 5.4 (black line). A dimer with a negative inter-planar angle is found to be the most stable configuration [Ahmed *et al.*, 2017]. Since dispersion forces are quantum mechanical long range attractive forces which result in the energy gain as the polarizability of one system interacts with the transition dipoles of the other, they are important for determining the equilibrium conformation and thermodynamics of many large molecules and van der Waal complexes [Antony *et al.*, 2015; Grimme, 2011]. Therefore, dispersion corrections are incorporated in the energy calculations. Using well established hybrid density functional method, B3LYP/6- 31G* [Becke, 1993; Petersson *et al.*, 1988; Petersson and Al-Laham, 1991] and PBE0 functional [Perdew *et al.*, 1996; Adamo and Barone, 1999] with Grimmes dispersion corrections [Antony *et al.*, 2015], single point energies are calculated for the geometry
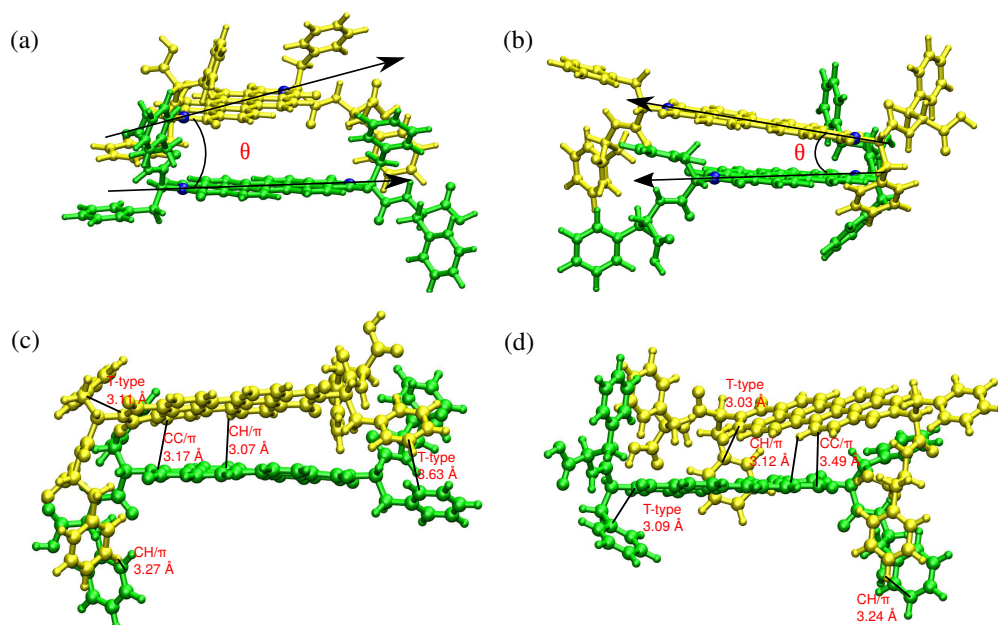
Figure 5.3: Initial snapshots of dimers with (a) positive inter-planar angle, (b) negative inter-planar angle. The inter-planar angle is the angle between the two vectors formed by joining the nitrogen atoms of the PDI cores. (c) RH and (d) LH (referred in figure 2) showing different stackings (CC/π or CH/π or T type π-interactions) with shortest distances.
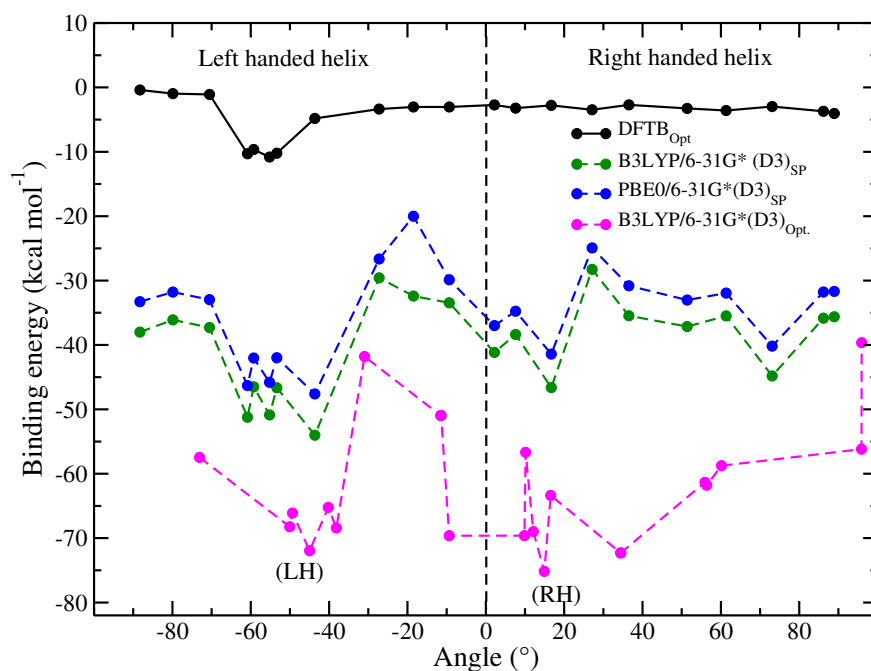

Figure 5.4: Stacking energies of P-1 dimers upon changing the inter-planar angle without and with dispersion corrections. (RH) and (LH) dimers correspond to anticlock-wise and clockwise inter-monomer rotations respectively.

optimized dimers and monomers obtained from DFTB using Gaussian 09 software [Frisch *et al.*, 2009]. Since the binding energies from DFTB full optimization (black line) and dispersion corrected

hybrid functional single point energies (green and magenta blue lines) differ significantly, the same configurations are fully optimized using DFT B3LYP/6-31G* considering dispersions corrections. These fully optimized geometries are used as the starting configurations for MD simulations.

5.2.2 Molecular dynamics simulations

The P-1 dimers with positive and negative inter-planar angles having strongest binding energies from the electronic structure calculations are referred to as RH and LH (in figure 5.4). These two configurations are used as the initial configurations for all-atom MD simulations. Each of the dimers is placed in a cubic box of dimensions of 4x4x4 nm^3. The bonded parameters are obtained from the fully optimized dimers, LH and RH. The force constants of bonded potentials are obtained from PRODRG [Schüttelkopf and van Aalten, 2004] and the partial charges are obtained from MOPAC charges using Automated Topology Builder (ATB) server [Malde *et al.*, 2011]. The bonded force-field parameters are available online in the reference [Srivastava *et al.*, 2020]. Non-bonded potentials are obtained from GROMOS54a7 [Schmid *et al.*, 2011] force-field using ATB. Each box is solvated with 980 SPC/E [Mark and Nilsson, 2001] water molecules to keep the water concentration closest to the experiment. A snapshot of the solvated positive and negative P-1 dimers is shown in figure 5.5(a) and (b) respectively. To keep the geometry obtained from the electronic structure
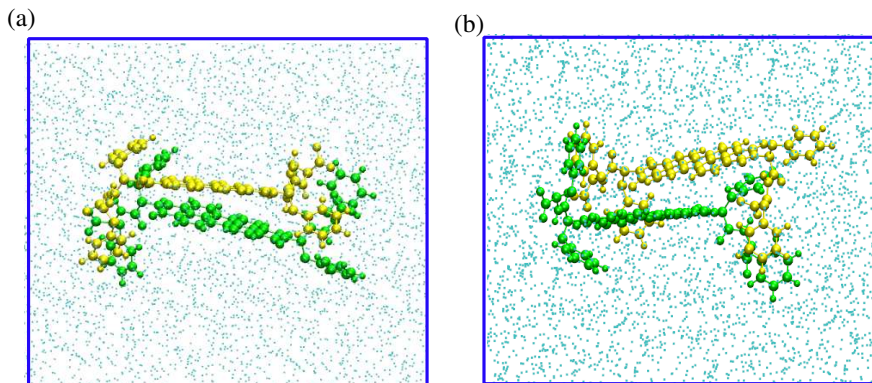

Figure 5.5: Snapshot of initial configurations of P-1 dimers with (a) positive inter-planar angle (RH) and (b) positive inter-planar angle (LH) solvated in water. Water molecules are shown in green color.

calculations intact in presence of water, all atoms of both the LH and RH dimers are positionally restrained by applying force constants of 1000 kJ mol^{-1} nm^{-2} in xyz directions. Both the solvated P-1 dimers (RH and LH) are energy minimization using steepest descent algorithm [Leach, 2001]. Next, 100 ps NVT simulations are carried out at 300 K using V-rescale thermostat [Bussi *et al.*, 2007a] followed by a 5 ns NPT run with a time step of 2 fs. V-rescale thermostat [Leach, 2001] and Berendsen barostat [Berendsen *et al.*, 1984] are used to maintain a constant temperature of 300 K and 1 bar pressure. The temperature and pressure coupling constants are 0.1 ps and 1 ps respectively. The Coulombic interactions are computed by using Particle Mesh Ewald method (PME) [Ewald, 1921]. The van der Waals interactions are cut-off at 1.2 nm. Periodic boundary conditions are applied along xyz.

Once the systems are equilibrated, the force constants for positional restrains are reduced to half and simulated again in an NPT ensemble under the same conditions. Next, 100 ns NPT simulations are carried out without positional restrains for both the dimers. Trajectories are collected at every 5 ps and the results are analyzed for 20000 frames. All simulations are carried out using GROMACS v2018 [Bekker *et al.*, 1993; Abraham *et al.*, 2018; Lindahl *et al.*, 2001; Berendsen *et al.*, 1995; van der Spoel *et al.*, 2005; Hess *et al.*, 2008; Pronk *et al.*, 2013; Páll *et al.*, 2015; Abraham *et al.*, 2015]. Further, simulations are also carried out for LH and RH dimers in

presence of 10% THF-water and pure THF respectively, similar to the experimental conditions. To obtain the parameters for THF, first it is geometry optimized using 6-31G* basis set. The bonded parameters for THF are taken from the ATB server and the non-bonded parameters are taken from the GROMOS54a7 force-field. The LH dimer is solvated with 930 SPC/E water molecules and 28 THF molecules to achieve the desirable solvent concentration of 10% THF-water. Similarly the RH dimer is solvated with 980 THF molecules to obtain 100 % THF concentration. Both the systems are energy minimized and simulated for 100 ps in an NVT ensemble, followed by an NPT simulation of 100 ns. The simulation parameters are kept same as the simulations of the dimers in pure water.

Next, we compute the potential of mean force (PMF) to understand the thermodynamic stability of the dimers in different solvents. This is carried out by performing the umbrella sampling simulations for both the LH and RH dimers in their respective solvents. The umbrella sampling is a biased method to overcome the sampling of unfavorable states. The biased potential energy obtained from the umbrella sampling is obtained by adding a biased potential $u_i(\xi)$ to the unbiased potential, given as [Kästner, 2011; Bochicchio $et\ al.$, 2015],

$$U^b(\mathbf{r}) \rightarrow U^u(\mathbf{r}) + u_i(\xi) \tag{5.4}$$

$$u_i(\xi) = \frac{1}{2}k(\xi - \xi_i)^2 \tag{5.5}$$

where $U^b(\mathbf{r})$ is the biased potential, $U^u(\mathbf{r})$ is the unbiased potential, $\mathbf{r}$ signifies a vector of all the coordinates, k is the force constant, ξ_i is the position along ξ around which enhanced sampling is performed. Umbrella sampling method requires N number of simulations, varied by ξ_i so that all the regions in the parameter space are sampled. This generates N overlapping histograms with a distribution function $P_i^b(\xi)$ which are biased due to the $u_i(\xi)$. Using these probability distributions, the potential of mean force is calculated using the weighted histogram analysis method. The unbiased probability distribution, $P_i^u(\xi)$ is determined [Kästner, 2011; Bochicchio $et\ al.$, 2015] from the biased distribution using the following equations,

$$P_i^b(\xi) = \frac{\int e^{-\beta[U(r)+u_i(\xi'(r))]}\delta[\xi'(r) - \xi]d^N r}{\int [e^-\beta(U(r) + u_i(\xi'(r)))]d^N r} \tag{5.6}$$

$$P_i^u(\xi) = P_i^b(\xi)e^{[\beta u_i(\xi)]} < e^{[-\beta u_i(\xi)]} > \tag{5.7}$$

Using the above equations, the unbiased free energy is computed as,

$$F_i(\xi) = -\frac{1}{\beta}lnP_i^b(\xi) - u_i(\xi) + f_i \tag{5.8}$$

where $f_i = -\frac{1}{\beta}ln < e^{-\beta u_i(\xi)} >$ and is independent of ξ.

To carry out the simulations, positional restrains are applied to one of the P-1 monomer and solvents and center of mass of the other P-1 is pulled along the z-direction, which is considered as the reaction coordinate ξ. Along with the positional restrains, rotational restrains are also applied to the P-1 molecules. The rotational potential is applied in the z-direction which is normal to the plane of P-1 monomer through the COM of the dimer. The functional form of the potential due to rotation restraint is given as [Hess $et\ al.$, 2008],

$$U_{rot} = \frac{k_{rot}}{2}\sum_{i=1}^{N}\frac{[(\hat{V} \times (x_i - x_a))\Omega(t)(y_i - y_a)]^2}{||\hat{V} \times (x_i - x_a)||^2 + \epsilon} \tag{5.9}$$

where k_{rot} is the rotational force constant, $\hat{V}$ is a unit vector parallel to the axis of rotation, x_i and y_i signify the current and the reference positions of ith-atom, x_a and y_a signify the current and the reference positions of COM of the atoms in each dimer, $\omega(t)$ is the rotation matrix and ϵ is a constant which is used to avoid singularity at the rotational axis.

The pulling simulation is carried out for 200 ps using a pulling rate of 0.01 nm ps^{-1} with a force constant of 5000 kJ mol^{-1} nm^{-2}. The initial COM distance between the P-1 monomers is 0.36 nm and 0.52 nm respectively for the LH and RH dimers, which are pulled upto 2.27 nm and 2.44 nm respectively. The temperature is maintained at 300 K using Nose-Hoover [Nosé, 1984] thermostat with a coupling constant of 1 ps. Next, different configuration windows are extracted for both the LH and RH dimers, each with a distance of 0.05 nm. Each configuration window is separately equilibrated for 100 ps in an NVT ensemble by removing the positional restrains on the solvent. For umbrella sampling, each equilibrated configuration is simulated for 10 ns and the trajectories hence obtained are processed for the analysis. The PMF is calculated by using the weighted histogram analysis method (WHAM).

5.3 RESULTS AND DISCUSSIONS

Experimental characterization

The synthesis of P-1 molecule was started by taking D- and L-phenylalanine amino acid. All the chemicals needed for preparing P-1 molecule were purchased from Sigma-Aldrich. The detailed synthetic route of P-1 is reported in reference [Ahmed *et al.*, 2017]. Self-assembled super-structure of P1-monomers is characterized by UV-vis spectroscopy obtained from Lambda 750 Perkin Elmer spectrophotometer. The UV-vis absorption spectra is shown in figure 5.6. The absorption peak at 500 nm is indicative of strong $\pi - \pi$ stacking interactions between aromatic core and side Phe rings present in P1 molecules.
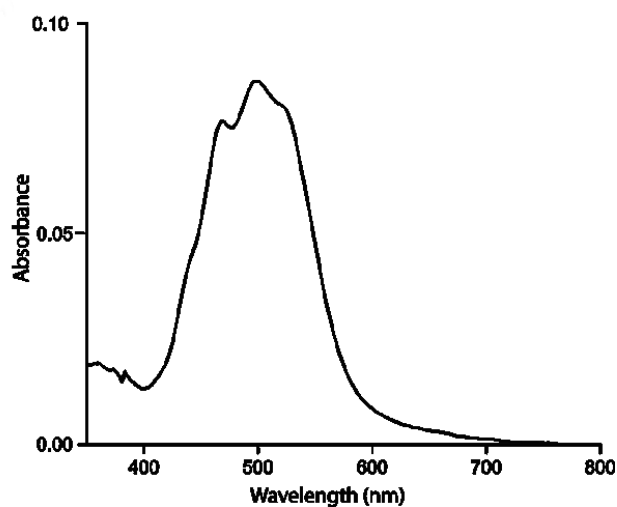

Figure 5.6: Normalized UV-vis absorption spectra obtained for 3% (7.5 μ M) THF-Water solvent. The absorption peak at 500 nm corresponds to $\pi - \pi$ stacking interactions between the P-1 monomers in the self-assembled super-structure.

Dispersion corrected binding energy

To understand the self-assembly process, binding energy of P1-dimers are computed using equation 5.3 and shown with respect to the inter-planar angle in figure 5.4. The most stable dimer from SCC-DFTB calculations is found at an angle of -55.20° with the binding energy of -10.81 kcal mol^{-1} (table 5.1) [Ahmed *et al.*, 2017]. Since the non-covalent aromatic interactions influence the conformations and the orientations of different moieties in space, the dimers are further

needed to optimize using dispersion corrections. To check the suitability of SCC-DFTB (D3) dispersion corrected method for the estimation of binding energies, we have calculated binding energy of a benzene dimer as a test case, using the same method. The benzene monomers are stacked at a distance of 3.9 Å forming a sandwiched structure. The binding energy turns out to be -4.57 kcal mol^{-1} (interplanar distance of 3.23 Å which is much stronger than the binding energies, 2.4-2.8 kcal mol^{-1} reported from single- and double-coupled cluster method using triple correction (CCSD(T)) calculations [Silva *et al.*, 2016] and 2.4 kcal mol^{-1} from experiment [Grover *et al.*, 1987]. Since SCC-DFTB (D3) results in an overestimation of binding energy of benzene dimer, dispersion corrected DFT with B3LYP and PBE0 functionals and 6-31G* basis sets are used to compute the binding energies of the geometry optimized P-1 dimers. The strongest binding energies are found to be -54.02 kcal mol^{-1} and -47.6 kcal mol^{-1} with B3LYP and PBE0 functionals respectively for the same conformer with an inter-planar angle of -43.6° at both levels of theories (figure 5.4). Previously, the binding energy of a PDI dimer with different side chains than the chains studied here is reported as -69.9 kcal mol^{-1} using DFT with M06-2X functional 6-31G (d) basis set [Chen *et al.*, 2015]. Since the binding energies obtained from the single point energy calculations are much less compared to the reported binding energies with similar moieties [Chen *et al.*, 2015], full geometry optimizations are carried out for all dimers using B3LYP/6-31G* considering dispersions corrections (D3). The strongest binding energy of -75.16 kcal mol^{-1} is found for a dimer with

Table 5.1: Binding energies (kcal mol^{-1}), angles (°) and distances (Å) for the RH and LH dimers. The results are compared with reported values for similar PDI analogues and PDI derivatives. [Ahmed *et al.*, 2017][a], [Oltean *et al.*, 2013][b], [Chen *et al.*, 2015][c].

System	Method used	Positive dimer			Negative dimer		
		Binding energy (ΔE_{BE})	Angle, θ (°)	Closest PDI distance	Binding energy (ΔE_{BE})	Angle, θ (°)	Closest PDI distance
P-1	SCC-DFTB[a]	-	-		-10.81	-55.2	2.89 (CH-π) 3.21 (CC-π)
	PBE0/6-31G*-(D3), single point	-47.61	-43.63	3.30 (CH-π) 3.48 (CC-π)	-41.41	16.71	3.94 (CH-π) 4.12 (CC-π)
	B3LYP/6-31G*-(D3), single point	-54.01	-43.63	3.3 (CH-π) 3.5 (CC-π)	-46.62	16.71	3.95 (CH-π) 4.03 (CC-π)
	B3LYP/6-31G*-(D3), optimization	-75.16	14.91	3.07 (CH-π) 3.17 (CC-π)	-71.96	-44.97	3.12 (CH-π) 3.49 (CC-π)
PTCDI[b]	PBE0-DCP/6-31+G(d, p)	ΔE_{BE}=-29.84 kcal mol^{-1}, θ=30.1°, Centroid distance=3.292 Å ΔE_{BE}=-25.57 kcal mol^{-1}, θ=0°, Centroid distance=4.893 Å					
BPTICNP-3[c]	M06-2X/6-31G(d), BSSE correction	ΔE_{BE}=-69.9 kcal mol^{-1} (syn conformation)					

the closest PDI distance of 3.07 Å (CH-π) and 3.17 Å (CC-π) and an inter-planar angle of 14.9° (table 5.1) with an anti-clockwise inter-planar rotation (figure 5.4, referred to as RH). The CH-π and CC-π type of non-covalent interactions are known to exhibit important roles in deciding the conformations of supra- structures and their functionalities [Mahadevi and Sastry, 2016]. The most stable dimer with clockwise or negative inter-planar angle is found at -44.97° (table 5.1) with a binding energy of -71.96 kcal mol^{-1} (referred to as LH in figure 5.4). For LH, the closest PDI distances are 3.12 Å (CH-π) and 3.49 Å (CC-π). These are very similar to the centroid distances (3.29 Å) at similar angle (30.1°) for PTCDI using PBE0-DCP/6-31+G(d, p) mentioned in table 5.1 [Oltean *et al.*, 2013]. The rugged nature of the binding energy with respect to the inter-planar angle in figure 5.4 appears due to allowing the molecules to undergo full geometry optimization without any restriction on the inter-planar distance or angle. The fully optimized RH and LH dimers are shown in figure 5.3 (c) and (d). For each configuration, CC-π, CH-π or T-type interactions with the shortest distance are presented. The binding energies of similar PDI analogues and derivatives (BPTICNP-3 Chen *et al.* [2015]) obtained from previous studies using M06-2X/6-31G(d) with BSSE correction agree well with the energies obtained from our calculations (table 5.1). In comparison to

the phenyl rings present in the P-1 monomer, BPTICNP-3 has a single cyanobenzene ring attached to the PDI core.

$\pi - \pi$ stacking distance calculations from MD

$\pi-\pi$ stacking interactions are indirectly determined using MD simulations as GROMOS54a7 force-field does not treat electrons explicitly. Our quantum calculations show that the aromatic moieties of P-1 should stay within 3.5 Å to exhibit $\pi - \pi$ stacking interactions. Similar distances are found from experiments as well [Ahmed *et al.*, 2017]. MD simulations of Perylenediimide DNA Base Surrogates considers a distance cut-off of ∼4.6 Å as $\pi-\pi$ interactions [Markegard *et al.*, 2015]. As the P-1 dimer is solvated in water during the MD simulations, the cut-off distance for $\pi - \pi$ interactions is considered as 4 Å.

The final configurations of the equilibrated dimers from MD simulations are shown in figure 5.7 (a), (b) where (a) and (b) refer to the RH and LH dimer in water respectively. Radial distribution
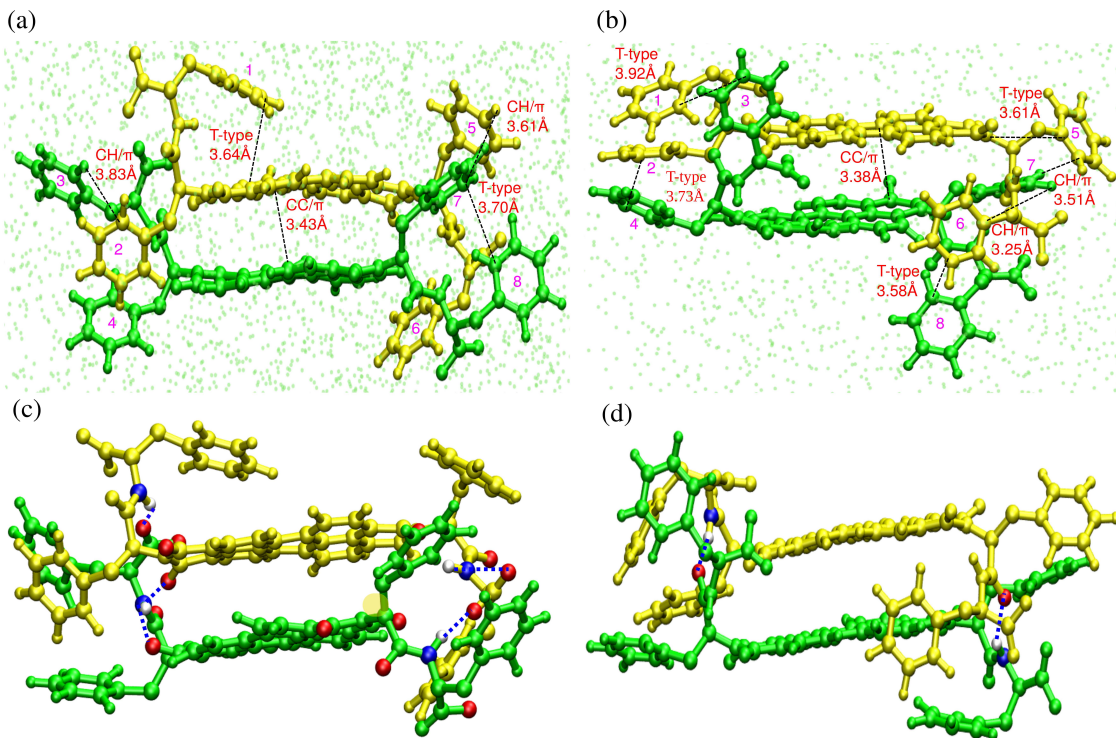

Figure 5.7: Snapshots of dimers with (a) positive inter-planar angle (RH) and (b) negative inter-planar angle (LH) from molecular dynamics simulations. Green dots: water. Side aromatic Phe rings in the P-1 molecule are labeled from 1-8. Snapshots of dimers with (c) positive and (d) negative inter-planar angle showing hydrogen bonding in P-1 dimers. Dotted black and blue lines represent π-stacking and hydrogen bonding respectively. Water are not shown for the sake of clarity.

function (RDF), g(r), of the center of mass (COM) of the PDI cores is calculated using the following equation,

$$g(r) = < \frac{1}{\rho N} \sum_{i=1}^{N} \sum_{j=1}^{N} \delta(r_{ij} - r) > \qquad (5.10)$$

where r_{ij} is the distance between the two particles i, j and N denotes the total number of particles, ρ signifies mean particle density. The angular brackets denote the averaging over all the times. The RDF plot is shown in figure 5.8. The most probable distance between the COM of the two PDI cores
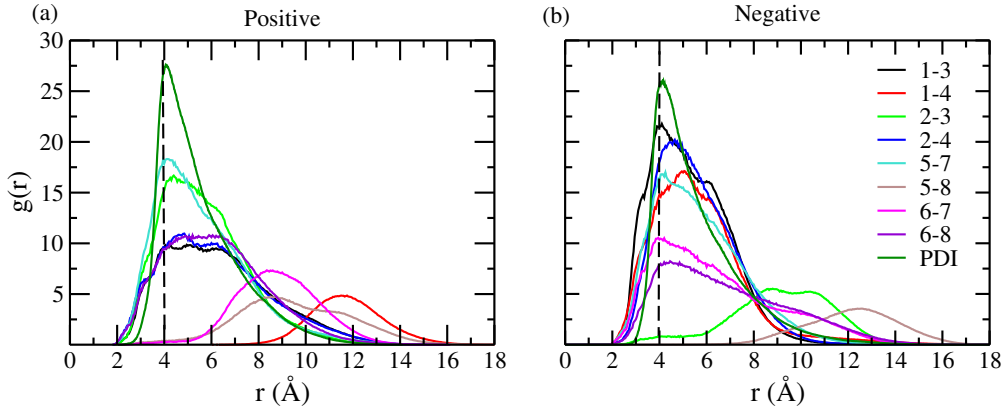
Figure 5.8: Radial distribution function, g(r), of the center of mass of PDI core and side rings (Phe motif) of dimers with (a) positive inter-planar angle, RH and (b) negative inter-planar angle, LH. Black dashed line denotes the distance for π-stacking interactions.

is found at $\sim$4 Å for both the dimers (dark solid green line in figure 5.8 and snapshots shown in figure 5.7 (a) and (b), which is similar to the distance between the COMs computed for Perylenediimide DNA Base Surrogates [Markegard *et al.*, 2015]. This distance refers to the $\pi-\pi$ stacking between the PDI cores of both RH and LH dimers. Additionally, intermolecular π-stackings are operative among the side aromatic Phe motifs labeled as 1 to 8 in figure 5.7 (a) and (b). The major contributions in intermolecular interactions of the dimer with positive inter-planar angle (RH) are from rings 5-7 and 2-3 (figure 5.8a), where the most probable distances between the COMs of these rings are within 4 Å corresponding to π-stacking. In comparison to this, higher extents of intermolecular π-interactions are found from 1-3, 5-7, 6-7 and 6-8 side Phe rings (shown in figure 5.7 (b) and 5.8 (b) of the negative inter-planar angle dimer (LH). The inter-planar angle constituted by two vectors joining C-C/N-N atoms across the Phe/PDI rings are shown schematically in figure 5.9. The rings which are within a distance of 4 Å (from the RDF) are considered for calculating the angular distributions to understand the orientations of the rings. The most probable angular distributions of the RH dimer is found at $\sim$45 ° (figure 5.9 a) whereas in the LH dimer, the interplanar angle of side aromatic rings show angle distributions near $\sim$20°, 100° and 160° (figure 5.9 (b)). All these orientations along with the COM distances obtained from the RDF confirm the presence of excess of T-type of intermolecular π-stacking interactions within the side aromatic rings of the dimer. The self-assembled P1-monomers show signatures of strong $\pi - \pi$ interactions characterized by UV-vis spectroscopy (figure 5.6). More intermolecular side Phe ring π-stacking interactions in the LH dimer compared to the RH dimer is facilitated by less probability of higher number of hydrogen bonding in the negative angle LH dimer (figure 5.7 (c) and (d) and figure 5.10). More numbers of hydrogen bonding in the RH dimer restrict the side Phe motifs to participate in π-stacking interactions. Thus, more π-stacking interactions of the Phe motifs in the LH dimer provide excess stability over the RH dimer.

Dimer energy from MD simulations

Electrostatic ($V_{Coulomb}$), van der Waals (V_{LJ}) and total non-bonded energies ($V_{Non-bonded}$) of both LH and RH dimers are calculated over 100 ns simulations using GROMACS. The total non-bonded energy is given as,

$$V_{Non-bonded} = V_{LJ} + V_{Coulomb} = 4\epsilon[(\frac{\sigma}{r})^{12} - (\frac{\sigma}{r})^6] + \frac{q_1 q_2}{4\pi\epsilon_0 r} \tag{5.11}$$

where σ denotes the distance of closest approach of two particles, ϵ is their interaction strength, ϵ_0 denotes permittivity of free space, $q_1 q_2$ is the product of charges of the particles and r denotes
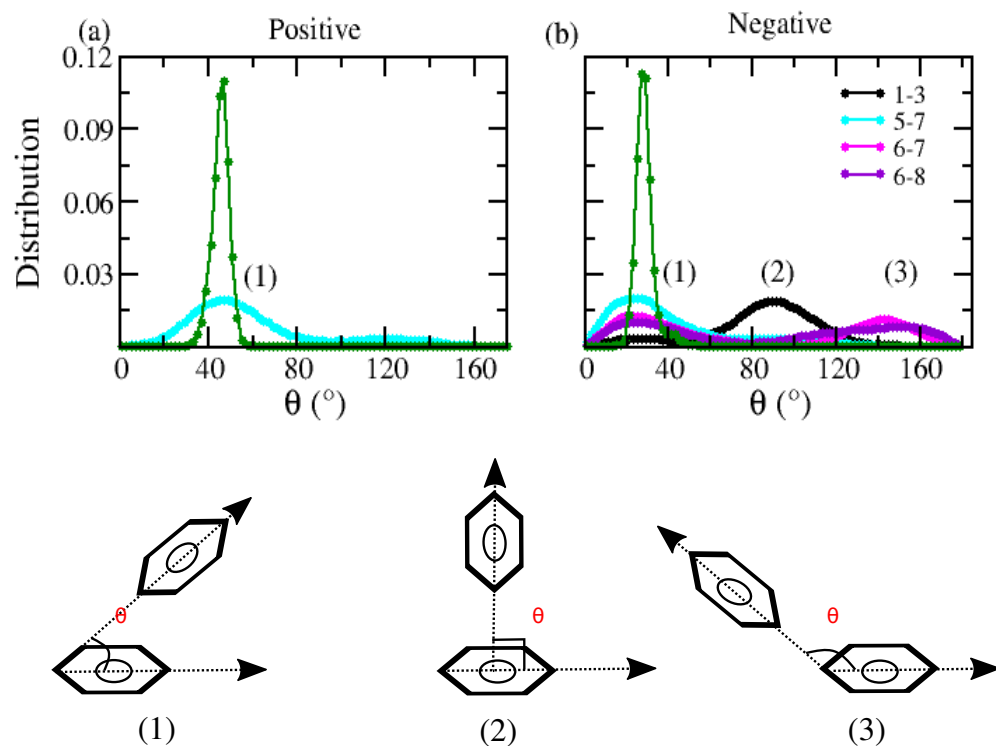
Figure 5.9: Distribution of inter-molecular angle for (a) positive inter-planar angle, RH and (b) negative inter-planar angle, LH dimers. Rings only within π-stackings are considered. The cartoon diagrams (1), (2) and (3) schematically show orientations of Phe motifs for π-stacking
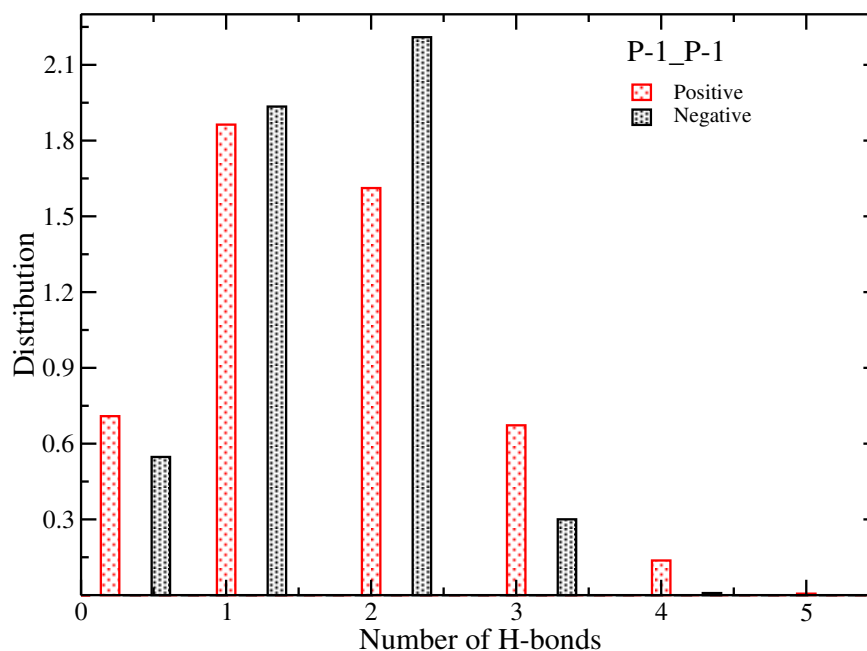

Figure 5.10: Distribution of hydrogen bonds formed in P-1 obtained from MD simulations for LH (negative) and RH (positive) interplanar angle dimer.

the distance between two particles. The probability distributions of these energies are shown in figure 5.11. Lower electrostatic (Coulombic) energies for the positive inter-planar angle dimer,
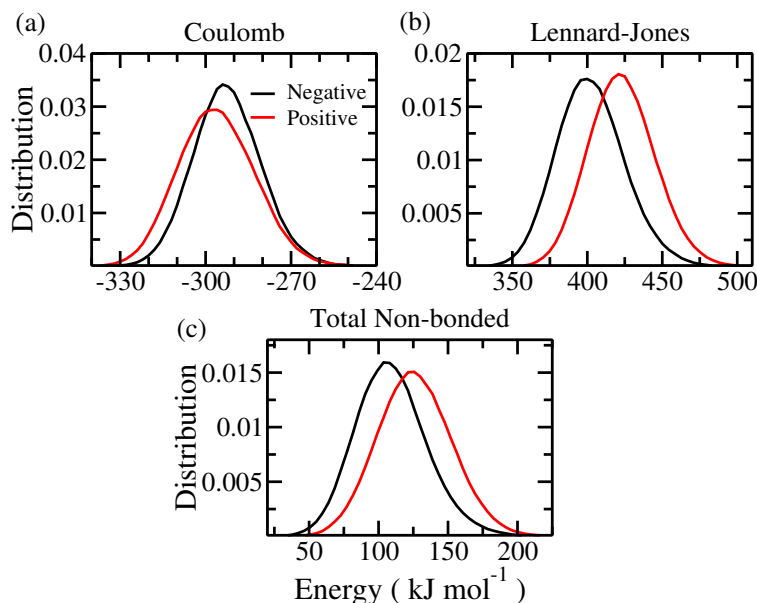

Figure 5.11: Distributions of non-bonded energies of dimer with positive (RH) and negative (LH) inter-planar angle. (a) Coulombic energy, (b) Lennard-Jones interaction energy and (c) total non-bonded potential energy.

RH (figure 5.11 a) is due to the presence of higher number of hydrogen bonds. On the other hand, energies from van der Waals (Lennard-Jones, figure 5.11 b) interactions are lower for the negative inter-planar angle LH dimer compared to the RH dimer. This is because of more π-stacking interactions of the Phe motifs in the LH dimer. The LH and RH dimers can act as the building blocks of the left and the right handed helical super structures by adopting a clockwise and an anti-clockwise arrangement, respectively. Lower non-bonded energy of the LH dimer (figure 5.11 c) accounts for energetically more favourable left handed helical super structure over the right handed one obtained by self-assembly of P-1 monomers. The non-bonded energies, closest distances and inter-planar angles of RH and LH dimers are reported under table 5.2. Previous experimental

Table 5.2: Non-bonded energies, closest distance and inter-planar angle of dimers with positive (RH) and negative (LH) inter- planar angle from molecular dynamics simulations.

		Positive Dimer (RH)	Negative Dimer (LH)
Energy $\times 10^2$ (kcal mol^{-1})	Lennard-Jones	4.21	4.0
	Coulomb	-2.97	-2.93
	Total non-bonded	1.23	1.07
Interplanar angle (°)		48.88	-25.57
Closest PDI distance (Å)		3.43	3.38
PDI COM distance (Å)		4.1	4.16
PDI COM distance, angle (MD simulation) [Huber *et al.*, 2014]		4.6±0.44 Å 15.51 ± 7.83°	

results [Ahmed *et al.*, 2017] have shown that in presence of THF, P-1 molecules self-assemble into nanofibers with right handed helicity. In presence of 10% THF-water, the left-handed nuclei of P-1 form thermodynamically stable nano-rings due to the restricted elongation of the nucleus into the fiber after a critical length. Thus we calculate potential of mean force of the LH and RH dimers to obtain the driving force behind the experimental findings [Ahmed *et al.*, 2017].

Potential of mean force (PMF)

The potential of mean force are calculated for both the LH and RH dimers from the umbrella sampling simulations using WHAM method using equation 5.8. The histograms of LH and RH dimers obtained after umbrella sampling simulations are shown in figure 5.12 which are further used to compute the PMF. To estimate the uncertainty in any quantity, the observations are repeated multiple times. The PMF calculated from WHAM method is based on 1001 trajectories, where each trajectory is obtained from a separate umbrella window. The histograms shown in figure 5.12 are the probability histograms along the reaction co-ordinate, ξ. For bootstrapping, 200 hypothetical histograms are chosen in a random manner from the given histograms which give a new histogram. Then, the new histogram is used in the WHAM method which gives a bootstrapped PMF. This process is repeated many times in order to obtain a large set of the bootstrapped PMFs. The error bars, which signify the standard deviation in the bootstrapped PMF is given by the equation,

$$\sigma_{PMF}(\xi) = [(N-1)^{-1} \sum_{i=1}^{N} (u_i(\xi) - <u_i(\xi)>)^2]^{(\frac{1}{2})} \tag{5.12}$$

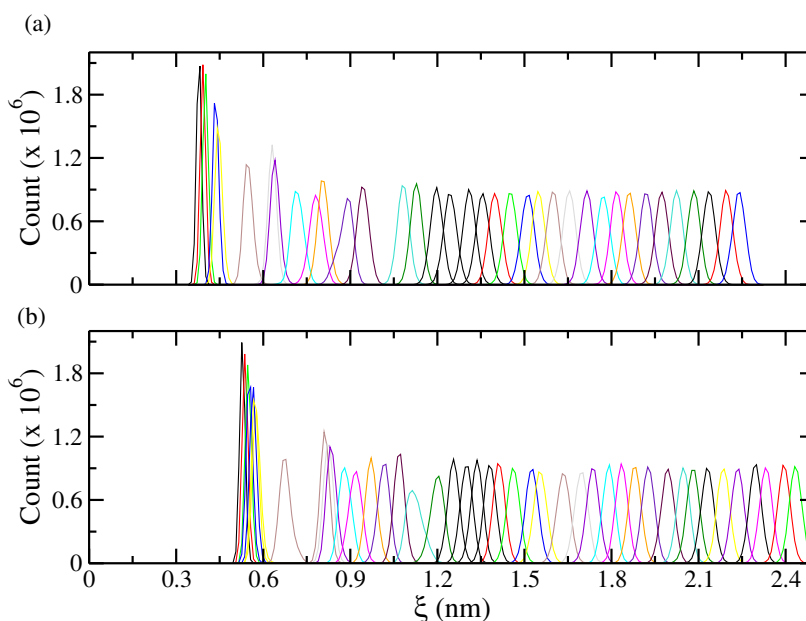where the quantity $<u_i(\xi)>$ measures the average PMF $(= \frac{1}{N} \sum_i^N u_i(\xi))$.

Figure 5.12: The overlapping histograms for (a) LH dimer and (b) RH dimer each obtained after 10 ns of umbrella sampling simulations in the presence of 10%THF-water and THF solvents respectively.

The PMFs of the LH and RH dimers (in 10% THF-water and THF respectively) along the reaction co-ordinate ξ are shown in figure 5.13, where the error bars represent the statistical uncertainty in the PMF. The error bars in the PMF is evaluated by using bootstrap analysis [Efron, 1979] using the gmx wham tool in GROMACS. The well-depths of the PMF of the two dimers are visible in the inset of the figure where the LH dimer in 10% THF-water has a lower depth compared to the RH one. The energy difference between the negative angle LH dimer (in 10% THF-water) and the positive angle RH dimer (in THF) is -933.77 cal mol^{-1}. Here the negative sign indicates the higher stability of the LH configuration over the RH configuration. The energy difference is higher than the energy at room temperature (597.26 cal mol^{-1}). This signifies that in order to change the helicity from a right-handed configuration to a left-handed configuration, there exists an energy barrier which is not achievable from the thermal energy. The dissociation energies of

the LH and RH dimers in their respective solvents are found to be 49.43 kcal mol^{-1} and 25.0 kcal mol^{-1} (figure 5.12). The dissociation energy of the LH dimer is approximately twice than that for the RH dimer, which makes the left-handed arrangement more stable. The snapshots of the dimers
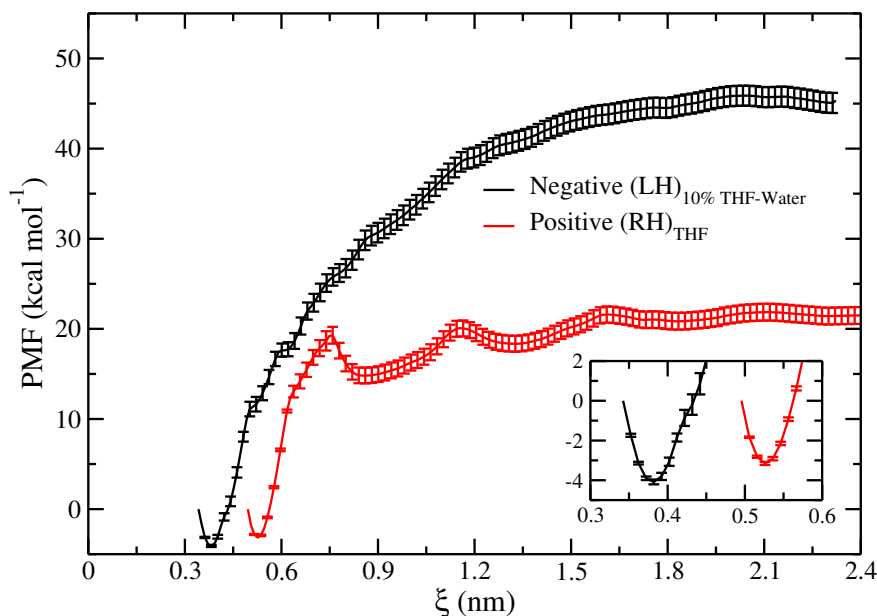

Figure 5.13: Potential of mean force (PMF) of dimer with negative (LH) and positive (RH) inter-planar angle in THF and 10% THF-water respectively. The inset shows the minima for them.

corresponding to the minimum PMF values are shown in figure 5.14. The closest distance between the PDI rings is 3.63 Å and 4.23 Å for the LH and RH dimers respectively. The $g(r)$ is calculated for both the PDI rings and the side rings in the LH and the RH dimers and is shown in figure 5.15. The PDI rings in both the dimers are located at a distance of ~4 Å which corresponds to the $\pi - \pi$ stacking distance. The side rings 1-3, 6-8 and 2-4 contribute effectively towards $\pi - \pi$ stacking in the LH dimer as their most probable locations are close to ~4 Å. However, only the side rings 2-4 in the RH dimer contributions towards $\pi - \pi$ stacking and the remaining rings are located beyond the required distance for the rings to participate in $\pi - \pi$ interactions. The side rings of the LH dimer interact via both T-type and H-type $\pi - \pi$ interactions, shown in figure 5.14 (a).

The hydrogen bond distribution for the LH and RH dimers in 10% THF-water and THF respectively is shown in figure 5.16. Both LH and RH dimers have the tendency to form intermolecular hydrogen bonds (shown in figure 5.14). The distribution shows that there is a slight difference in the number of hydrogen bonds in the LH and RH dimers. Thus the stability of the LH dimer in 10%THF-water is attributed to higher extent of $\pi - \pi$ interactions between the PDI core and the side aromatic rings. The radial distribution function of solvents near the PDI core and the side rings are shown in figure 5.17. The distribution of THF is distinctly high near both the PDI core and side rings in the LH dimer, whereas a broad and uniform THF distribution exists near the rings in the RH dimer. Polar water molecules prefer to stay away from the aromatic PDI rings of the LH dimer. The THF molecules are less polar than water and hence they prefer to stay near the non-polar PDI core and side rings of both the dimers. Due to the presence of solvents with opposite polarities in 10% THF-water, the non-polar rings prefer to stay away from water and interact among themselves via $\pi - \pi$ interactions (shown in figure 5.14(a)), which is assisted by the less polar THF molecules. On the other hand, there is no competitive solvent effect in the RH dimer as it contains only THF molecules. Thus a wide and uniform distribution of THF is seen near the PDI and side rings (figure 5.17 (a)). Thus, the solvent plays an important role in the preferential configuration of the dimers where the competitive polarities of the solvents assist in the specific
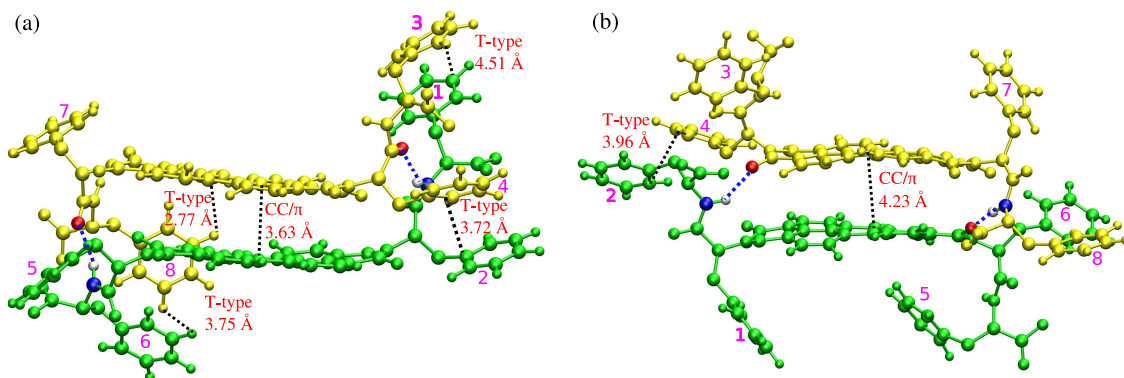
Figure 5.14: Snapshots of (a) negative (LH) and (b) positive (RH) dimer corresponding to the configurations with minimum potential of mean force obtained from umbrella sampling simulations in the presence of 10% THF-water and THF respectively (figure 5.13 inset). Dotted black and blue lines represent π-stacking and hydrogen bonding respectively. Solvent molecules are omitted for the sake of clarity.
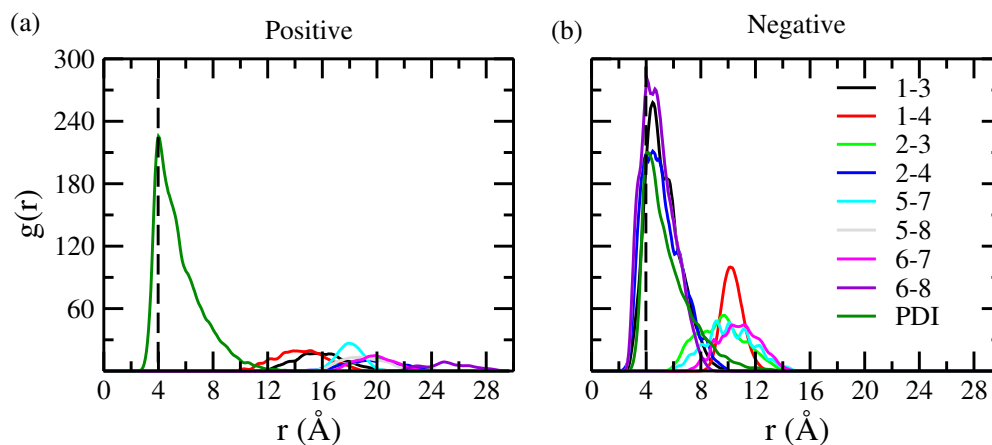

Figure 5.15: Radial distribution function ($g(r)$) of PDI rings and side aromatic rings in (a) positive (RH) dimer in pure THF and (b) negative (LH) dimer in presence of 10% THF-water.

orientations and stability of the structures. Thus the LH dimer in 10%THF-water is stable over the RH dimer in THF due to higher $\pi - \pi$ interactions. Thus, more non-covalent interactions and higher dissociation energy of the LH dimer in 10% THF-water compared to the RH dimer in pure THF makes it a thermodynamically stable arrangement over the RH dimer. As mentioned earlier, previous experiment has shown that the right handed helical fibres in THF changes to nanorings in 10% THF water. This is because the building blocks of the right handed helical fibres are the RH dimers which have less dissociation energy and less PMF compared to the LH dimers which can be the building blocks of the nanorings. This analysis infers the selectivity of a left handed arrangement over the right handed one using different solvents and provides an understanding to the experimental findings [Ahmed *et al.*, 2017].
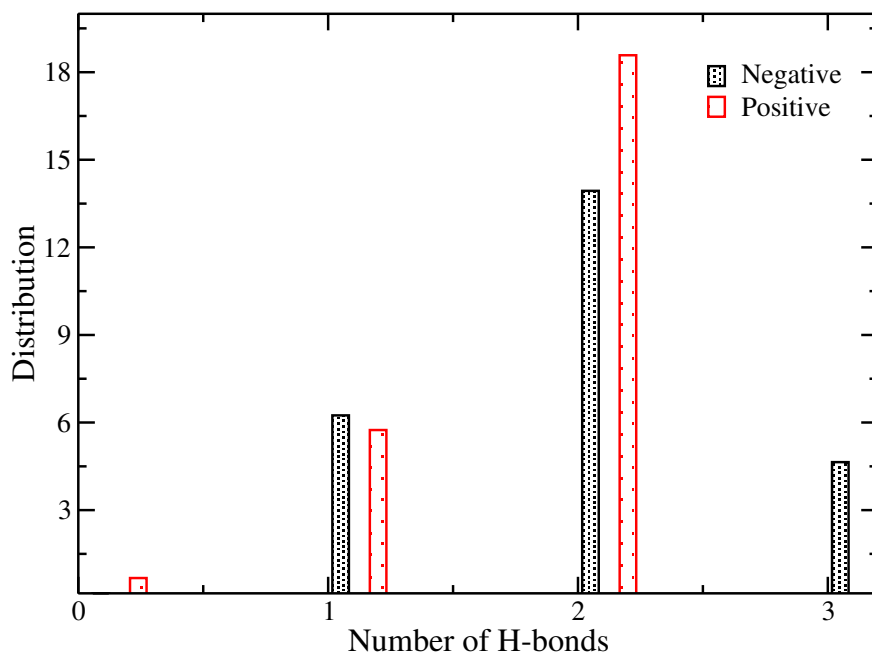
Figure 5.16: Hydrogen bond distribution in LH and RH dimers in the presence of 10% THF-water and pure THF solvents.

5.4 SUMMARY AND CONCLUSIONS

Binding energies and the stability of parallel sliced dimers of a π-conjugated molecule, P-1, have been investigated using electronic structure calculations and molecular dynamics simulations. Experiments conducted earlier on self-assembly of P-1 [Ahmed *et al.*, 2017] show the role of ring orientations on the morphology of the aggregated structure exhibiting semi-conducting properties. In THF, P-1 monomers self-assemble into right handed helical fibers, which turn into thermodynamically stable nano-rings from a left-handed helical nucleation site in THF/water [Ahmed *et al.*, 2017]. To explain the observation, binding energies of P-1 dimers with positive and negative inter planar angles are calculated using SCC-DFTB, DFT-D3 PBE0/6-31G* and B3LYP/6-31G* methods. Without dispersion corrections, the binding energy of the most stable dimer is found to be -10.81 kcal mol^{-1} [Ahmed *et al.*, 2017]. Using dispersion interactions, the most stable dimer is formed at an angle of 14.92 ° with binding energy of -75.16 kcal mol^{-1}. MD simulations in water show that the LH dimer with negative inter-planar angle has higher stability compared to the dimer with positive inter-planar angle and can be the nucleation site of a left handed helix. This is due to excess T-type inter and intra-molecular π-stacking interactions present in the aromatic Phe-Phe motifs of the LH P-1 dimer. The absorption spectrum of self-assembled P1 monomers in THF-water confirms the presence of π-stacking interactions. This is consistent with stronger Lennard-Jones interactions and weaker Coulombic interactions in the LH dimer compared to the other when both solvated in pure water. Umbrella sampling simulations are carried out for the LH and RH dimers in the presence of 10% THF-water and THF respectively to obtain the PMF and dissociation energies. The LH dimer in 10% THF-water has lower PMF and higher dissociation energy than the RH dimer in THF. Thus the formation of the LH dimer in 10% THF-water is thermodynamically controlled and the formation of the RH dimer in 100% THF is kinetically controlled. The high intermolecular $\pi - \pi$ interactions in 10% THF-water are responsible for the stability of the negative angle LH dimer. Thus, the solvent plays an important role in the preferential geometries of the P-1 dimer systems. The more stable LH dimer with a negative inter-planar angle over the RH dimer can act as a nucleation site of a super structure of nanoring as seen in the previous experiment. The analysis provides an explanation of the experiments performed earlier
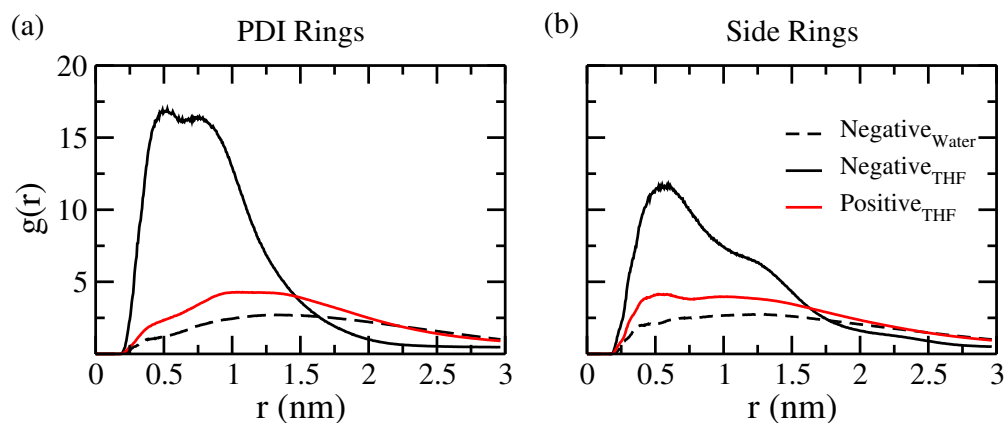
Figure 5.17: Radial distribution function of water and THF near (a) PDI rings and (b) side rings for the negative (LH) and positive (RH) dimers.

and can be extended to study the self-assembly of higher order units like trimer, tetramer using advanced sampling techniques. This has future applications in the fields of bio-active materials, synthetic receptors or in designing the building blocks of supra-structure based devices.

Publications:
1. Sahnawaz Ahmed, Bapan Pramanik, K. N. Amba Sankar, Abhinav Srivastava, Nilotpal Singha, Payel Dowari, **Arpita Srivastava**, Kallol Mohanta, Ananya Debnath and Debapratim Das, Solvent Assisted Tuning of Morphology of a Peptide-Perylenediimide Conjugate: Helical Fibers to Nano-Rings and their Differential Semiconductivity **2017**, Scientific Reports, *9485*, 1.
2. **Arpita Srivastava**, Avinash Garg, Debapratim Das and Ananya Debnath, Molecular dynamics simulations of a stacked π-conjugated soft material: binding energy and preferential geometry for self-assembly **2020**, Bulletin of Materials Science (Invited for Thematic issue on Soft Materials), *43*, 1.